Understanding the Measurement Range of Single-axis Force-rebalance MEMS Vibratory Gyroscopes

Yanhui Jiang

School of Mechanical Engineering, Nanjing University of Science and Technology;
Xuanwu, Nanjing, 210094, China

Email: jyhnl@njust.edu.cn

Abstract

Micro-electromechanical system (MEMS) vibratory gyroscopes are inertial sensors for measuring angular velocity based on a micro-machined proof-mass that can detect rotating-induced inertial force (i.e., Coriolis force). During the past several decades, great advancement has been achieved in the fields of design and fabrication of MEMS vibratory gyroscopes, however, little investigation on understanding and improving their measurement range could be found in the literature. We find that most of the commercial single-axis force-rebalance MEMS vibratory gyroscopes have a measurement range of the order $10^{2}{}^{\circ}/\mathrm{s}$. A question naturally arises: is there any physical reasoning to the limit of the measurement range? To answer this question, we propose a theoretical method to investigate the limit by creating a mathematical model for typical single-axis force-rebalance MEMS vibratory gyroscopes. A deeper analysis gives the answer to the question, for the first time.

Keywords: MEMS; Gyroscope; Centrifugal force; Measurement range; Force-rebalance

1. Introduction

Micro-electromechanical system (MEMS) vibratory gyroscopes are inertial sensors for measuring angular velocity based on a micro-machined proof-mass that can detect rotating-induced inertial force (i.e., Coriolis force) [1, 2]. They are widely used in consumer electronics, automobiles and other modern engineering products [3-5] due to their light weight, small volume, low cost, and ease of integration.

During the past several decades, great advancement has been achieved in the fields of design and fabrication of MEMS vibratory gyroscopes [6]. Nevertheless, most of the achievements is about how to improve the measurement accuracy, especially after the navigation-grade Boeing Disc gyroscope emerged [7]. In contrast, little investigation on understanding and improving their measurement range could be found, while abundant test data about the measurement range of various designs are available.

For several typical commercial single-axis MEMS vibratory gyroscopes that work under a force-rebalance mode, we see that SCR2100-D08 (Murata Inc.) has a measurement range $125°/s$, ADXR453 (Analog Devices Inc.) has a measurement range $300°/s$, GYPRO4300 (Tronics Inc.) has a measurement range $300°/s$, and CRH02-100 (Silicon Sensing Inc.) has a measurement range $100°/s$. It shows that their measurement ranges are all of the order $10^{2}°/s$. A question naturally arises: is there any physical reasoning to the limit of the measurement range?

Herein, we present a mathematical method to answer the above question. While the

commercial single-axis force-rebalance MEMS vibratory gyroscopes may have different proof-mass structures (e.g., axially symmetric rings/multi-rings, discs), their motion could be described by a general lumped parameter model in terms of mass, damping coefficient, and stiffness of the proof-mass [8]. It is noted that the gyroscopes with multiple proof-masses are beyond the scope of this article.

2. Theory and formulations

Consider a proof-mass whose mass is denoted as m on a rotatory table. To describe its motion, a co-rotating Cartesian coordinate system O-xyz is established with the origin denoted as O and the three basis vectors denoted as $\{\mathbf{i},\mathbf{j},\mathbf{k}\}$. The basis vectors $\{\mathbf{i},\mathbf{j}\}$ expand the x-y plane of the rotatory table. The angular velocity $\Omega\mathbf{k}$ of the rotatory table is constant and orthogonal to the x-y plane. The proof-mass is initially rest at the origin. Therefore, the position vector of the proof-mass is

$$\mathbf{r} = \mathrm{x}\mathbf{i} + \mathrm{y}\mathbf{j} \tag{1}$$

The velocity of the proof-mass is

$$\dot{\mathbf{r}} = \left(\dot{\mathrm{x}} - \Omega\mathrm{y}\right)\mathbf{i} + \left(\dot{\mathrm{y}} + \Omega\mathrm{x}\right)\mathbf{j} \tag{2}$$

The acceleration of the proof-mass is

$$\ddot{\mathbf{r}} = \left(\ddot{\mathrm{x}} - 2\Omega\dot{\mathrm{y}} - \Omega^2\mathrm{x}\right)\mathbf{i} + \left(\ddot{\mathrm{y}} + 2\Omega\dot{\mathrm{x}} - \Omega^2\mathrm{y}\right)\mathbf{j} \tag{3}$$

The motion of the proof-mass is constrained by a viscous force.

$$\mathbf{f}_{\text{Viscous}} = -\mathrm{c}\dot{\mathrm{x}}\mathbf{i} - \mathrm{c}\dot{\mathrm{y}}\mathbf{j} \tag{4}$$

and an elastic force

$$\mathbf{f}_{\text{Elastic}} = -\text{kx}\mathbf{i} - \text{ky}\mathbf{j} \tag{5}$$

where we assume the damping coefficient c and the stiffness k are constant when the proof-mass moves relative to the rotatory table along any radial direction from the origin.

Per Newton's law of motion, the equation of motion is stated as

$$\text{m}\ddot{\mathbf{r}} = \mathbf{f}_{\text{Viscous}} + \mathbf{f}_{\text{Elastic}} + \mathbf{f}_{\text{External}} \tag{6}$$

where $\mathbf{f}_{\text{External}} = \text{f}_\text{x}\mathbf{i} + \text{f}_\text{y}\mathbf{j}$ denotes the external force exerted on the proof-mass.

Introducing Eq. (3), (4), and (5) into Eq. (6), one obtain the equation of motion in the non-inertial co-rotating frame as

$$\begin{cases} \text{m}\ddot{\text{x}} + \text{c}\dot{\text{x}} + \text{kx} = \text{f}_\text{x} + 2\Omega\text{m}\dot{\text{y}} + \Omega^2\text{mx} \\ \text{m}\ddot{\text{y}} + \text{c}\dot{\text{y}} + \text{ky} = \text{f}_\text{y} - 2\Omega\text{m}\dot{\text{x}} + \Omega^2\text{my} \end{cases} \tag{7}$$

where the centrifugal force is identified as

$$\mathbf{f}_{\text{Centrifuge}} = \Omega^2\text{mx}\mathbf{i} + \Omega^2\text{my}\mathbf{j} \tag{8}$$

and the Coriolis force

$$\mathbf{f}_{\text{Coriolis}} = 2\Omega\text{m}\dot{\text{y}}\mathbf{i} - 2\Omega\text{m}\dot{\text{x}}\mathbf{j} \tag{9}$$

Eq. (7) clearly shows that the centrifugal force lowers down the stiffness of the system, and the Coriolis force couples the two original independent degrees of freedom x and y.

When the system is subjected to a harmonic load, the equation of motion is

$$\begin{cases} \text{m}\ddot{\text{x}} + \text{c}\dot{\text{x}} + \text{kx} = \text{f}_{\text{xc}}\cos\omega\text{t} + \text{f}_{\text{xs}}\sin\omega\text{t} + 2\Omega\text{m}\dot{\text{y}} + \Omega^2\text{mx} \\ \text{m}\ddot{\text{y}} + \text{c}\dot{\text{y}} + \text{ky} = \text{f}_{\text{yc}}\cos\omega\text{t} + \text{f}_{\text{ys}}\sin\omega\text{t} - 2\Omega\text{m}\dot{\text{x}} + \Omega^2\text{my} \end{cases} \tag{10}$$

where f_{xc}, f_{xs}, f_{yc} and f_{ys} are the amplitudes of the cosine and sine components of the load, and ω is the circular frequency of the load. Dividing both sides of Eq. (10) by

m, one obtains

$$\begin{cases} \ddot{x} + 2\xi\omega_n \dot{x} + \omega_n^2 x = F_{xc}\cos\omega t + F_{xs}\sin\omega t + 2\Omega\dot{y} + \Omega^2 x \\ \ddot{y} + 2\xi\omega_n \dot{y} + \omega_n^2 y = F_{yc}\cos\omega t + F_{ys}\sin\omega t - 2\Omega\dot{x} + \Omega^2 y \end{cases} \tag{11}$$

where $\omega_n = \sqrt{k/m}$ is the natural frequency, $\xi = c/c_{cr} \geq 0$ is the damping ratio, $c_{cr} = 2\sqrt{mk}$ is the critical damping, $F_{xc} = f_{xc}/m$ $F_{xs} = f_{xs}/m$, $F_{yc} = f_{yc}/m$, and $F_{ys} = f_{ys}/m$.

We assume the solution to Eq. (11) takes the following form

$$\begin{cases} x = c_x\cos\omega t + s_x\sin\omega t \\ y = c_y\cos\omega t + s_y\sin\omega t \end{cases} \tag{12}$$

where c_x, s_x, c_y and s_y are unknown coefficients to be determined. From Eq. (12), the velocity is

$$\begin{cases} \dot{x} = -c_x\omega\sin\omega t + s_x\omega\cos\omega t \\ \dot{y} = -c_y\omega\sin\omega t + s_y\omega\cos\omega t \end{cases} \tag{13}$$

The acceleration is

$$\begin{cases} \ddot{x} = -c_x\omega^2\cos\omega t - s_x\omega^2\sin\omega t \\ \ddot{y} = -c_y\omega^2\cos\omega t - s_y\omega^2\sin\omega t \end{cases} \tag{14}$$

Introducing Eq. (12), Eq. (13), and Eq. (14) into Eq. (11), one has

$$\begin{bmatrix} \omega_n^2 - \omega^2 - \Omega^2 & 2\xi\omega_n\omega & 0 & -2\Omega\omega \\ -2\xi\omega_n\omega & \omega_n^2 - \omega^2 - \Omega^2 & 2\Omega\omega & 0 \\ 0 & 2\Omega\omega & \omega_n^2 - \omega^2 - \Omega^2 & 2\xi\omega_n\omega \\ -2\Omega\omega & 0 & -2\xi\omega_n\omega & \omega_n^2 - \omega^2 - \Omega^2 \end{bmatrix} \begin{bmatrix} c_x \\ s_x \\ c_y \\ s_y \end{bmatrix} = \begin{bmatrix} F_{xc} \\ F_{xs} \\ F_{yc} \\ F_{ys} \end{bmatrix} \tag{15}$$

Furthermore, dividing both sides of Eq. (15) by ω_n^2, one arrives at

$$\begin{bmatrix} 1-\lambda^2-\kappa^2 & 2\xi\lambda & 0 & -2\kappa\lambda \\ -2\xi\lambda & 1-\lambda^2-\kappa^2 & 2\kappa\lambda & 0 \\ 0 & 2\kappa\lambda & 1-\lambda^2-\kappa^2 & 2\xi\lambda \\ -2\kappa\lambda & 0 & -2\xi\lambda & 1-\lambda^2-\kappa^2 \end{bmatrix} \begin{bmatrix} c_x \\ s_x \\ c_y \\ s_y \end{bmatrix} = \begin{bmatrix} u_{xc} \\ u_{xs} \\ u_{yc} \\ u_{ys} \end{bmatrix} \tag{16}$$

where $u_{xc} = F_{xc}/\omega_n^2 = f_{xc}/k$, $u_{xs} = f_{xs}/k$, $u_{yc} = f_{yc}/k$, and $u_{ys} = f_{ys}/k$ are called static displacements that characterize the amplitudes of the load, $\lambda = \omega/\omega_n$ is the frequency ratio, ξ is the damping ratio, and $\kappa = \Omega/\omega_n > 0$ is the normalized rotational speed. These three non-dimensional parameters determine the steady state response of the system.

The solution could be explicitly stated as

$$\begin{bmatrix} c_x \\ s_x \\ c_y \\ s_y \end{bmatrix} = \frac{1}{E} \begin{bmatrix} A & -B & D & C \\ B & A & -C & D \\ -D & -C & A & -B \\ C & -D & B & A \end{bmatrix} \begin{bmatrix} u_{xc} \\ u_{xs} \\ u_{yc} \\ u_{ys} \end{bmatrix} \tag{17}$$

where

$$\begin{aligned} A &= \alpha\left(\alpha^2+\beta^2-\chi^2\right) \\ B &= \beta\left(\alpha^2+\beta^2+\chi^2\right) \\ C &= \chi\left(\alpha^2-\beta^2-\chi^2\right) \\ D &= 2\alpha\beta\chi \\ E &= \alpha^4+\beta^4+\chi^4+2\alpha^2\beta^2+2\beta^2\chi^2-2\alpha^2\chi^2 \\ \alpha &= 1-\lambda^2-\kappa^2 \\ \beta &= 2\xi\lambda \\ \chi &= 2\kappa\lambda \end{aligned} \tag{18}$$

We design a harmonic load per the requirement of the force-rebalance working mode widely adopted in single-axis MEMS vibratory gyroscopes, namely, letting $u_{xc} = 0$,

$u_{xs} > 0$, $u_{yc} = 0$, and $u_{ys} = 0$. Since damping is required to be controlled to a very small value in an ideal gyroscope, we thus assume the damping effect is negligible (i.e., $\beta = 0$).

From Eq. (17) and Eq. (18), we have

$$\begin{aligned} A &= \alpha\left(\alpha^2 - \chi^2\right) \\ B &= 0 \\ C &= \chi\left(\alpha^2 - \chi^2\right) \\ D &= 0 \\ E &= \left(\alpha^2 - \chi^2\right)^2 \end{aligned} \tag{19}$$

and

$$\begin{bmatrix} c_x \\ s_x \\ c_y \\ s_y \end{bmatrix} = \frac{u_{xs}}{\alpha^2 - \chi^2} \begin{bmatrix} 0 \\ \alpha \\ -\chi \\ 0 \end{bmatrix} \tag{20}$$

Introducing Eq. (20) into Eq. (12), the steady state response of the system is therefore derived as

$$\boxed{\begin{cases} \bar{x} = \dfrac{u_{xs}\alpha}{\alpha^2 - \chi^2}\sin\omega t \\ \bar{y} = -\dfrac{u_{xs}\chi}{\alpha^2 - \chi^2}\cos\omega t \end{cases}} \tag{21}$$

In practice, the steady state response $\bar{x}$ is also called the drive mode, and the steady state response $\bar{y}$ is called the detection mode.

3. Results and Discussions

From Eq. (21), we have the following conclusions:

(1) The drive mode is of the same phase angle with the harmonic load, while the detection mode has a phase difference of $-\frac{\pi}{2}$.

(2) The amplitude of the detection mode is not proportional to the angular speed.

$$\bar{y} = -\frac{u_{xs}\chi}{\alpha^2 - \chi^2} = -\frac{2\lambda u_{xs}\Omega}{\omega_n\left(1-\lambda^2-\left(\Omega/\omega_n\right)^2\right)^2 - \left(2\lambda\right)^2\left(\Omega/\omega_n\right)^2} \not\propto \Omega \tag{22}$$

See the solid lines plotted in **Fig.1** for $\lambda = 0.7, 0.8, 0.9$ based on Eq. (22).

(3) When the normalized rotational speed is small $\kappa << 1$, (i.e., $\Omega << \omega_n$) and the higher order terms of κ is negligible (i.e., $\kappa^2 = 0$), one has the following relationship

$$\begin{aligned} &\bar{y} = -\frac{u_{xs}\chi}{\alpha^2 - \chi^2} \\ &\overset{\kappa \ll 0}{\Rightarrow} \\ &\hat{y} = -\frac{u_{xs}\chi}{\left(1-\lambda^2\right)^2} = -\frac{2u_{xs}\lambda\Omega}{\omega_n\left(1-\lambda^2\right)^2} \propto \Omega \end{aligned} \tag{23}$$

where $\alpha^2 - \chi^2 = \left(1-\lambda^2-\kappa^2\right)^2 - \left(2\kappa\lambda\right)^2$. Eq. (23) lays the theoretical foundation for the force-rebalance working principle of an ideal vibratory gyroscope. See the dashed lines (linearized) plotted in **Fig.1** for $\lambda = 0.7, 0.8, 0.9$ based on Eq. (23). It is obvious that the dashed lines and solid lines are overlapped when κ is small. In addition, it shows that a larger frequency ratio λ indicates a smaller measurement range.

(4) From Eq. (23), we see that, by tuning the driving frequency close to the natural frequency or increasing the load u_{xs}, one can improve the scaling factor (SF) for an ideal gyroscope.

$$SF = \frac{|\hat{y}|}{\Omega} = \frac{1}{\omega_n} \frac{2u_{xs}\lambda}{\left(1-\lambda^2\right)^2} \tag{24}$$

When resonance takes place $\lambda = 1$, the SF will go to infinity (i.e., $SF \to \infty$) since damping effect is neglected.

(5) Consider the deviation between Eq. (22) and Eq. (23)

$$DEV = \frac{|\overline{y}| - |\hat{y}|}{u_{xs}} = \frac{\chi}{\left|\alpha^2 - \chi^2\right|} - \frac{\chi}{\left(1-\lambda^2\right)^2} \tag{25}$$

If a deviation bound (DB) is specified (i.e., letting DEV<=DB=1E-3) and a frequency ratio $0 < \lambda < 1$ is also specified, by Eq. (25), one is able to determine a critical point $\kappa_{Critical}$ beyond which the deviation will exceed the DB (e.g., DB=1E-3). As an extension to **Fig.1**, **Fig.2** shows how the critical point is determined for a given DB and a given λ. When DB is constant (e.g., see **Fig.2a** DB=1E-3), a relationship between the critical point $\kappa_{Critical}$ and the frequency ratio λ could be plotted as a critical line. **Fig.2b** and **Fig.2c** show the cases for DB=1E-2 and DB=1E-1, respectively. It is noted that a smaller DB means a better degree of linearity of the gyroscopes.

Therefore, the measurement range could be determined by this critical point as following (i.e., the maximum rotational speed within a specified degree of linearity)

$$\Omega_{Max} = \kappa_{Critical}\omega_n \tag{26}$$

Fig.3 plots out the critical point $\kappa_{Critical}$ as a function of the frequency ratio λ for three different DBs (i.e., 1E-3, 1E-4, and 1E-5). The function is nonlinearly decreasing as λ changes from 0 to 1. For a larger DB, the critical point $\kappa_{Critical}$ value will be larger for a

specific λ. As the frequency ratio λ approximates 1 (i.e., approaching a resonant frequency) per the requirement of the force-rebalance working mode for detection purpose, the order of the critical point κ_{Critical} value is 10^{-4}, as shown in **Fig. 3**.

$$\kappa_{\text{Critical}} \sim 10^{-4} \tag{27}$$

On the other hand, for most of the commercial single-axis force-rebalance MEMS vibratory gyroscopes, the natural frequency ω_n of their proof-masses is around the order $10^4\,\text{Hz}$ [9]

$$\omega_n \sim 10^4\,\text{Hz} \tag{28}$$

Introducing Eq. (27) and Eq. (28) into Eq. (26), one has

$$\Omega_{\text{Max}} \sim 1\text{Hz} \sim 10^{2}{}^{\circ}/\text{s} \tag{29}$$

Thus, we demonstrate that most of the commercial single-axis force-rebalance MEMS vibratory gyroscopes have a measurement range of the order $10^{2}{}^{\circ}/\text{s}$.

Reference

1. Yazdi, N., F. Ayazi, and K. Najafi, *Micromachined inertial sensors.* Proceedings of the IEEE, 2002. **86**(8): p. 1640-1659.
2. Acar, C. and A. Shkel, *MEMS vibratory gyroscopes: structural approaches to improve robustness*. 2009: Springer.
3. Aggarwal, P., Z. Syed, and N. El-Sheimy, *MEMS-based integrated navigation*. 2010: Artech House.
4. Hommel, M., H. Knab, and S.G. Yousef, *Reliability of automotive and consumer MEMS sensors-An overview.* Microelectronics Reliability, 2021. **126**: p. 114252.
5. Fanse, T.S., *Micro-electro-mechanical system (MEMS) application and prospects in automobile.* IOSR J. Mech. Civ. Eng, 2022. **19**: p. 17-21.
6. Stanimirović, Z. and I. Stanimirović, *Advanced MEMS Technologies.* Microelectromechanical Systems (MEMS)-Innovation, Manufacturing Techniques and Applications: Innovation, Manufacturing Techniques and Applications, 2025: p. 7.
7. Challoner, A.D., et al., *Boeing Disc Resonator Gyroscope,* in *2014 Ieee/Ion Position, Location and Navigation Symposium - Plans 2014*. 2014. p. 504-514.
8. Lynch, D.D. *Vibratory gyro analysis by the method of averaging*. in *Proc. 2nd St. Petersburg Conf. on Gyroscopic Technology and Navigation*. 1995.
9. Liewald, J.-T., et al., *100 kHz MEMS vibratory gyroscope.* Journal of Microelectromechanical systems, 2013. **22**(5): p. 1115-1125.

Acknowledgement

The author thanks the financial support from the Science and Technology Commission (Grant No. 2021-JCJQ-JJ-XXXX) and Jiangsu Province (Grant No. JSSCBS20210205) of the PRC.

Competing interests

Author declares that they have no competing interests.

Fig. 1

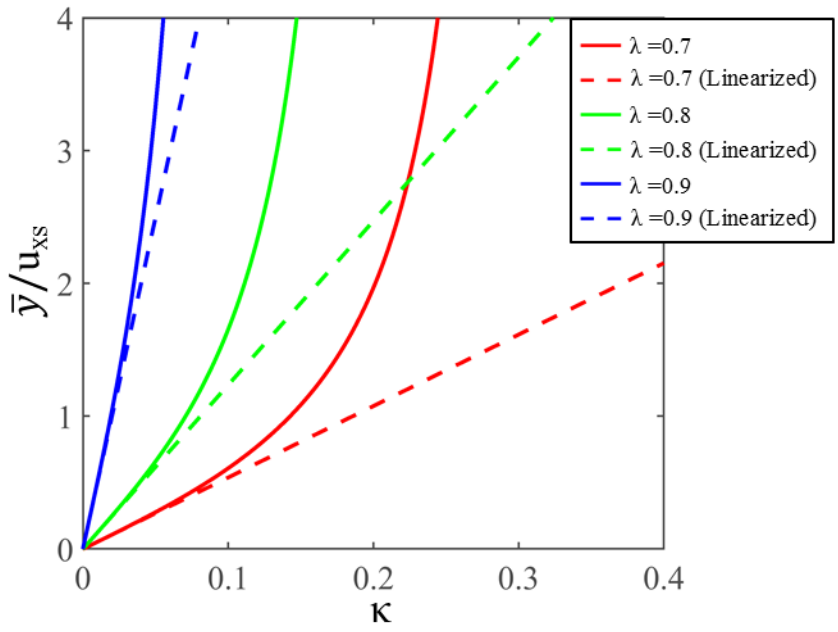

Plots of the normalized amplitude of detection mode as a function of the normalized rotational speed κ for three different frequency ratios λ (i.e., 0.7, 0.8, and 0.9)

Fig.2

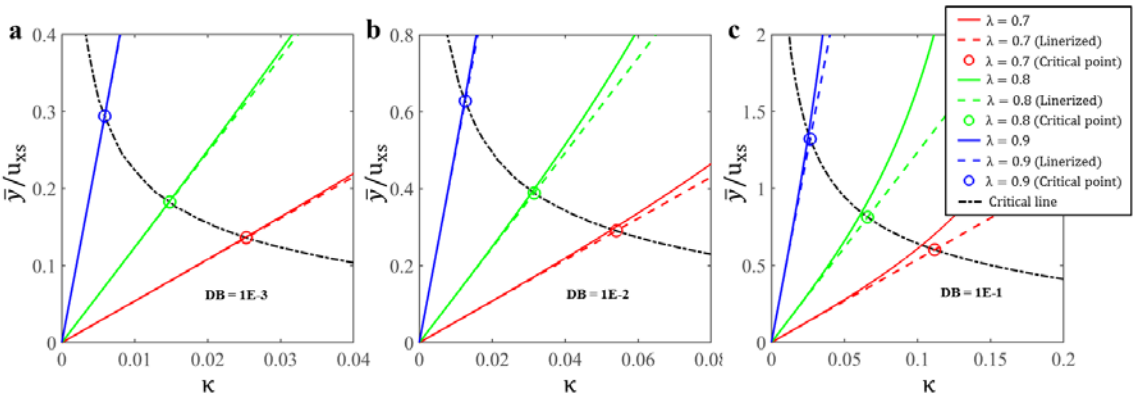

Plots based on Fig.1 of the critical points and lines for three different DBs (a) DB=1E-3 (b) DB=1E-2 (c) DB=1E-1

Fig. 3

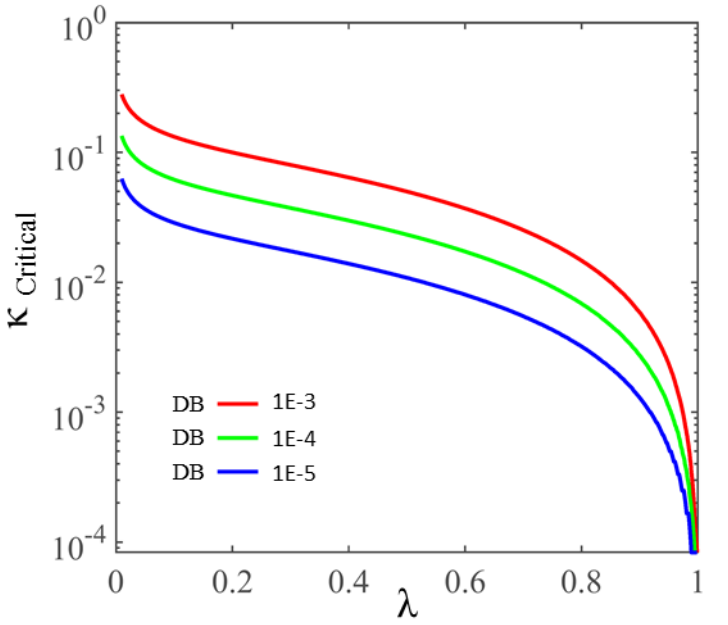

Plots of the critical point $\kappa_{Critical}$ as a function of the frequency ratio λ for three different DBs (i.e., 1E-3, 1E-4, and 1E-5)